

Phonon-assisted Kondo Effect in a Single-Molecule Transistor out of Equilibrium

Zuo-Zi Chen¹, Haizhou Lu¹, Rong Lü¹ and Bang-fen Zhu^{1,2}

¹ Center for Advanced Study, Tsinghua University, Beijing 100084, P. R. China

² Department of Physics, Tsinghua University, Beijing 100084, P. R. China

E-mail: zzchen@castu.tsinghua.edu.cn, bfzhu@castu.tsinghua.edu.cn

Abstract. The joint effect of the electron-phonon interaction and Kondo effect on the nonequilibrium transport through the single molecule transistor is investigated by using the improved canonical transformation scheme and extended equation of motion approach. Two types of Kondo phonon-satellites with different asymmetric shapes are fully confirmed in the spectral function, and are related to the electron spin singlet or hole spin singlet, respectively. Moreover, when a moderate Zeeman splitting is caused by a local magnetic field, the Kondo satellites in the spin resolved spectral function are found disappeared on one side of the main peak, which is opposite for different spin component. All these peculiar signatures that manifest themselves in the nonlinear differential conductance, are explained with a clear physics picture.

PACS numbers: 72.15.Qm, 85.65.+h, 73.63.Kv, 71.38.-k

1. Introduction

The Kondo effect as a manifestation of strongly correlations between conduction electrons and spin impurity has been extensively studied in the context of quantum dot physics in past years. [1–7] Recently, its realization in the single-molecule transistor (SMT) has attracted a lot of attentions. [8–14] In particular, the latest experiments in SMT, in which the phonon satellite has been clearly observed even in the Kondo regime [15–17] owing to the enhanced electron-vibration coupling in the molecule, [18–20] has stimulated great interests to investigate the interplay of the electron-phonon interaction (EPI) and the Kondo effect on the transport through the SMT.

According to our recent investigation on the spectral function of the SMT in the absence of the Coulomb interaction, the phonon satellites are quite sensitive to the lead Fermi levels with respect to the localized level. [21] When the temperature is too low to excite phonons thermally, the phonon satellites can only develop below (above) the resonant level if this level is occupied (empty) initially, as then electrons can only emit phonons. On the other hand, in the Kondo regime with the EPI ignored, it is well known that two collective spin singlet states will be formed between the localized state and the excited electron states above the Fermi level μ or the excited hole states below μ because of spin exchange processes, [22, 23] which will contribute to the formation of the sharp Kondo peak pinning at the Fermi surface in the local density of states. It is thus expected that the interesting transport physics may result from the interplay of both the EPI and the Kondo effect, in particular out of the equilibrium, as both effects are sensitive to the Fermi levels at the source and drain electrode.

Several theoretical techniques have been developed and applied to address the joint effects of the EPI and the Kondo correlation on transport through a quantum dot or a SMT. [24–34] According to these works, the equilibrium properties, in particular the renormalized effect on the Kondo correlation due to the EPI, have been well described. For example, with the help of the numerical renormalization group approach, the renormalized effect has been predicted for wide range of parameters in the equilibrium. [26–29] With the help of generalized Schrieffer-Wolff transformation, under the assumption that the system stays equilibrium in the strongly asymmetric coupling case, the nonlinear differential conductance has been given in Ref. [30] with the Kondo satellite structure exhibited. On the other hand, owing to the lack of satisfactory treatment for the nonequilibrium Kondo problem, little effort has been made to investigate how the Kondo phonon-satellites develop and manifest themselves in the nonequilibrium transport. However, since the Kondo phonon-satellites can only be observed at finite bias voltage experimentally, when the system is driven out of equilibrium, [15–17] it is certainly of importance to investigate the key signature of the nonequilibrium phonon-Kondo effect. As far as we know, by the real-time diagrammatic formulation, Köning et al. have given the spectral function as well as the differential conductance with Kondo satellites in the nonequilibrium situation. [24, 25] Here we shall develop another easier and straightforward approach, which will combine the

improved nonperturbative canonical transformation treatment of the EPI [21] with the extended equation-of-motion (EOM) method of the nonequilibrium Green functions. This approach, although is not rigorous in quantitative description, has the advantage of intuitiveness and can provide a semi-quantitative understanding of the phonon-assisted Kondo effect, particularly for strong electron-vibration coupling as well as nonequilibrium situation.

Based on the approach mentioned above, in the present paper, we shall mainly focus on how the Kondo satellites develop and manifest themselves in the nonequilibrium transport through the SMT, and how these Kondo satellites are affected by an applied local magnetic field. After the Introduction we shall give our model and method in Section II and III, respectively. Our main results are presented in Section IV, which include: (i) The Kondo phonon-satellites may exhibit quite different asymmetric line-shapes with respect to the Kondo main peak in the spectral function, and also in the nonlinear differential conductance; (ii) Two types of spin exchange processes, associated with the collective spin singlets formed by electron states and by hole states respectively, can be clearly distinguished by the Kondo satellites; and (iii) With a moderate Zeeman splitting exceeded the width of Kondo peak, its Kondo-phonon satellites only appear on one side of the main Kondo peak in one spin-resolved spectral function, and on the opposite side for the opposite spin component. Finally, the conclusions are drawn.

2. Model

The SMT system studied in the present paper can usually be described as the Anderson-Holstein model, in which a single localized state coupled linearly to one local vibration mode and to the left (L) and right (R) non-interacting leads, namely

$$\begin{aligned} \mathbf{H} = & \sum_{\alpha;\mathbf{k},\sigma} \varepsilon_{\alpha\mathbf{k}} \mathbf{c}_{\alpha\mathbf{k}\sigma}^\dagger \mathbf{c}_{\alpha\mathbf{k}\sigma} + \sum_{\sigma} \varepsilon_{\sigma} \mathbf{n}_{\sigma} + U_0 \mathbf{n}_{\uparrow} \mathbf{n}_{\downarrow} + \hbar\omega_0 \mathbf{a}^\dagger \mathbf{a} \\ & + \sum_{\sigma} \lambda \mathbf{n}_{\sigma} (\mathbf{a}^\dagger + \mathbf{a}) + \sum_{\alpha;\mathbf{k},\sigma} (V_{\alpha\mathbf{k}} \mathbf{c}_{\alpha\mathbf{k}\sigma}^\dagger \mathbf{d}_{\sigma} + h.c.), \end{aligned} \quad (1)$$

where $\mathbf{c}_{\alpha\mathbf{k}\sigma}^\dagger (\mathbf{c}_{\alpha\mathbf{k}\sigma})$ and $\mathbf{d}_{\sigma}^\dagger (\mathbf{d}_{\sigma})$ are the creation (annihilation) operators for the lead electron with energy $\varepsilon_{\alpha\mathbf{k}}$ and the localized SMT electron with energy ε_{σ} , respectively, σ denotes the spin index and the lead index $\alpha = L, R$. U_0 is the on-site Coulomb repulsion, and $\mathbf{n}_{\sigma} = \mathbf{d}_{\sigma}^\dagger \mathbf{d}_{\sigma}$. The operator \mathbf{a}^\dagger (\mathbf{a}) creates (annihilates) the local vibration mode with frequency ω_0 , λ is the EPI strength, $V_{\alpha\mathbf{k}}$ is the tunneling coupling between the localized and lead electrons, which results in a level broadening $\Gamma = (\Gamma_L + \Gamma_R)/2$, where

$$\Gamma_{\alpha}(\omega) \equiv 2\pi \sum_{\mathbf{k}} |V_{\alpha\mathbf{k}}|^2 \delta(\omega - \varepsilon_{\alpha\mathbf{k}}). \quad (2)$$

To treat the EPI non-perturbatively, by the canonical transformation, $\mathbf{S} = \frac{\lambda}{\omega_0} \sum_{\sigma} \mathbf{n}_{\sigma} (\mathbf{a}^\dagger - \mathbf{a})$, the Hamiltonian is transformed into $\bar{\mathbf{H}} \equiv e^{\mathbf{S}} \mathbf{H} e^{-\mathbf{S}} = \bar{\mathbf{H}}_{ph} + \bar{\mathbf{H}}_{el}$, where the phonon part $\bar{\mathbf{H}}_{ph} = \hbar\omega_0 \mathbf{a}^\dagger \mathbf{a}$, and the electron part turns out to be the

Anderson Hamiltonian, namely

$$\begin{aligned} \bar{\mathbf{H}}_{el} = & \sum_{\alpha, \mathbf{k}, \sigma} \varepsilon_{\alpha \mathbf{k}} \mathbf{c}_{\alpha \mathbf{k} \sigma}^\dagger \mathbf{c}_{\alpha \mathbf{k} \sigma} + \sum_{\sigma} \bar{\varepsilon}_{\sigma} \mathbf{n}_{\sigma} + \bar{U}_0 \mathbf{n}_{\uparrow} \mathbf{n}_{\downarrow} \\ & + \sum_{\alpha, \mathbf{k}, \sigma} (\bar{V}_{\alpha \mathbf{k}} \mathbf{c}_{\alpha \mathbf{k} \sigma}^\dagger \mathbf{d}_{\sigma} + h.c.). \end{aligned} \quad (3)$$

The parameters with bar in Eq.(3) correspond to the renormalized ones resulted from the canonical transformation, e.g., the SMT level is shifted to $\bar{\varepsilon}_{\sigma} = \varepsilon_{\sigma} - g\omega_0$ with $g \equiv (\lambda/\omega_0)^2$, and the on-site repulsion is renormalized to $\bar{U}_0 = U_0 - 2g\omega_0$. When the charging energy is significantly reduced by screening due to the electrodes, [35] \bar{U}_0 may become negative for very strong EPI, which will result in the anisotropic Kondo effect. [26–29] But in most realistic situations, the charging energy is much larger than the EPI energy, [18–20] so we shall limit ourselves to the standard Kondo effect, i.e. \bar{U}_0 remains positive. Besides, $\bar{V}_{\sigma \mathbf{k}} \equiv V_{\sigma \mathbf{k}} \mathbf{X}$ with $\mathbf{X} \equiv \exp [-(\lambda/\omega_0) (\mathbf{a}^\dagger - \mathbf{a})]$, indicating that a cloud of phonons will be created or destroyed during the hopping processes. As containing the phonon operator \mathbf{X} , the renormalized Hamiltonian $\bar{\mathbf{H}}_{el}$ has not been fully decoupled. For the present work, we are specially interested in the cases where the EPI is sufficiently strong compared to the tunneling coupling so that a local polaron is formed. Then we can approximate the phonon operator \mathbf{X} by its expectation value in the thermal equilibrium, $\langle \mathbf{X} \rangle = \exp [-g (N_{ph} + 1/2)]$, with N_{ph} defined as the population of phonons at temperature T . Although it belongs to the mean field approximation, this method has been used widely and obtained reasonable successes. [36–41]

With this mean field approximations, the lesser Green function can then be separated into the electron part and phonon part,

$$\begin{aligned} G_{\sigma}^{<}(t) \equiv & i \langle \mathbf{d}_{\sigma}^{\dagger}(0) \mathbf{d}_{\sigma}(t) \rangle = i \langle \bar{\mathbf{d}}_{\sigma}^{\dagger} e^{i\bar{\mathbf{H}}t} \bar{\mathbf{d}}_{\sigma} e^{-i\bar{\mathbf{H}}t} \rangle \\ = & i \langle \mathbf{d}_{\sigma}^{\dagger} e^{i\bar{\mathbf{H}}_{el}t} \mathbf{d}_{\sigma} e^{-i\bar{\mathbf{H}}_{el}t} \rangle_{el} \langle \mathbf{X}^{\dagger} e^{i\bar{\mathbf{H}}_{ph}t} \mathbf{X} e^{-i\bar{\mathbf{H}}_{ph}t} \rangle_{ph}. \end{aligned} \quad (4)$$

The trace of the phonon part can be evaluated by the Feynman disentangling technique. [39] The lesser Green function of the SMT electron can be decoupled as

$$G_{\sigma}^{<}(\omega) = \sum_{n=-\infty}^{\infty} L_n \bar{G}_{\sigma}^{<}(\omega + n\omega_0), \quad (5)$$

and similarly the greater Green function is formulated as

$$G_{\sigma}^{>}(\omega) = \sum_{n=-\infty}^{\infty} L_n \bar{G}_{\sigma}^{>}(\omega - n\omega_0). \quad (6)$$

Here $\bar{G}_{\sigma}^{>(<)}$ is the dressed Green function associated with $\bar{\mathbf{H}}_{el}$, and

$$L_n = e^{-g(2N_{ph}+1)} e^{n\omega_0/2k_B T} I_n \left(2g\sqrt{N_{ph}(N_{ph}+1)} \right), \quad (7)$$

in which $I_n(z)$ is the n -th Bessel function of complex argument. The spectral function is then calculated with the lesser and greater Green functions via

$$A_{\sigma}(\omega) = i(G_{\sigma}^{>}(\omega) - G_{\sigma}^{<}(\omega)). \quad (8)$$

It should be emphasized that people usually evaluate the spectral function via $A_\sigma(\omega) = i(G_\sigma^r(\omega) - G_\sigma^a(\omega))$, in which the retarded and advanced Green functions, G_σ^r and G_σ^a , are approximately separated into the electron and phonon parts by ignoring the difference between the N_{ph} and $N_{ph} + 1$, which works only in the high-temperature limit. [36–38] However, the phonon-Kondo problem studied here is certainly not the case, as the characteristic Kondo temperature, T_K , is very low. Hence the prescription we have recently made may be more appropriate [21].

3. Keldysh Green functions

Within the Keldysh formalism, the dressed Green functions $\bar{G}_\sigma^{>(<)}$ can be derived from $\bar{\mathbf{H}}_{el}$ with the help of the EOM approach. Since the usual approximation in decoupling the higher-order Green functions generated by EOM is valid only nearby or above the Kondo temperature T_K , [42, 43] at lower temperature as in the present situation the approximation developed by Lacroix may be more appropriate [44]. In the original Lacroix approach, only the system with the spin degeneracy and infinite charging energy was discussed in the equilibrium. To apply to the nonequilibrium situation with the finite U_0 and Zeeman splitting, we have extended it accordingly. Thus, the usually ignored higher-order retarded Green function are taken into reconsideration. For example, $\langle\langle \mathbf{d}_{\bar{\sigma}} \mathbf{c}_{\alpha\mathbf{k}\bar{\sigma}}^\dagger \mathbf{c}_{\alpha'\mathbf{k}'\sigma}, \mathbf{d}_\sigma^\dagger \rangle\rangle$ is now approximately decoupled as $\langle \mathbf{d}_{\bar{\sigma}} \mathbf{c}_{\alpha\mathbf{k}\bar{\sigma}}^\dagger \rangle \langle\langle \mathbf{c}_{\alpha'\mathbf{k}'\sigma}, \mathbf{d}_\sigma^\dagger \rangle\rangle$, and the matrix element $\langle \mathbf{d}_{\bar{\sigma}} \mathbf{c}_{\alpha\mathbf{k}\bar{\sigma}}^\dagger \rangle$ should be determined self-consistently by the nonequilibrium Green function technique.

From the standard derivation of the EOM, [45, 46] the dressed retarded Green function turns out to be

$$\begin{aligned} \bar{G}_\sigma^r(\omega) = & \frac{1 - (\langle \bar{\mathbf{n}}_{\bar{\sigma}} \rangle + \bar{P}_{\bar{\sigma}}(\bar{\omega}_\sigma^0) + \bar{P}_{\bar{\sigma}}^*(-\bar{\omega}^U))}{\omega - \bar{\varepsilon}_\sigma - \bar{\Sigma}^{(T)}(\omega) + \frac{\bar{U}_0 \bar{\Sigma}_{\bar{\sigma}}^{(1)}(\omega)}{\omega - \bar{\varepsilon}_\sigma - \bar{U}_0 - \bar{\Sigma}^{(T)}(\omega) - \bar{\Sigma}_{\bar{\sigma}}^{(3)}(\omega)}} \\ & + \frac{\langle \bar{\mathbf{n}}_{\bar{\sigma}} \rangle + \bar{P}_{\bar{\sigma}}(\bar{\omega}_\sigma^0) + \bar{P}_{\bar{\sigma}}^*(-\bar{\omega}^U)}{\omega - \bar{\varepsilon}_\sigma - \bar{U}_0 - \bar{\Sigma}^{(T)}(\omega) - \frac{\bar{U}_0 \bar{\Sigma}_{\bar{\sigma}}^{(2)}(\omega)}{\omega - \bar{\varepsilon}_\sigma - \bar{\Sigma}^{(T)}(\omega) - \bar{\Sigma}_{\bar{\sigma}}^{(3)}(\omega)}}, \end{aligned} \quad (9)$$

where

$$\begin{aligned} \bar{\omega}_\sigma^0 & \equiv \omega + \bar{\varepsilon}_\sigma - \bar{\varepsilon}_\sigma, \\ \bar{\omega}^U & \equiv \omega - \bar{\varepsilon}_\sigma - \bar{\varepsilon}_{\bar{\sigma}} - \bar{U}_0, \end{aligned} \quad (10)$$

and the correlation function between the SMT level and leads, $\bar{P}_{\bar{\sigma}}(\omega)$, is defined as

$$\bar{P}_{\bar{\sigma}}(\omega) \equiv \sum_{\alpha\mathbf{k}} \bar{V}_{\alpha\mathbf{k}}^* \langle \mathbf{d}_{\bar{\sigma}}^\dagger \mathbf{c}_{\alpha\mathbf{k}\bar{\sigma}} \rangle g_{\alpha\mathbf{k}}^r(\omega), \quad (11)$$

in which $g_{\alpha\mathbf{k}}^r(\omega)$ is the unperturbed retarded Green function of the lead electron. In the above the self-energy associated with the resonant tunneling processes is defined as

$$\bar{\Sigma}^{(T)}(\omega) \equiv \sum_{\alpha\mathbf{k}} |\bar{V}_{\alpha\mathbf{k}}|^2 g_{\alpha\mathbf{k}}^r(\omega), \quad (12)$$

and the self-energies related to the Kondo correlation are respectively expressed as

$$\begin{aligned}\bar{\Sigma}_{\bar{\sigma}}^{(1)}(\omega) &= \bar{\Sigma}_{\bar{\sigma}}^{(0)}(\omega) - \bar{\Sigma}^{(T)}(\omega) [\bar{P}_{\bar{\sigma}}(\bar{\omega}_{\bar{\sigma}}^0) + \bar{P}_{\bar{\sigma}}^*(-\bar{\omega}^U)], \\ \bar{\Sigma}_{\bar{\sigma}}^{(3)}(\omega) &= \bar{\Sigma}^{(T)}(\bar{\omega}_{\bar{\sigma}}^0) - (\bar{\Sigma}^{(T)}(-\bar{\omega}^U))^*, \\ \bar{\Sigma}_{\bar{\sigma}}^{(2)}(\omega) &= \bar{\Sigma}_{\bar{\sigma}}^{(3)}(\omega) - \bar{\Sigma}_{\bar{\sigma}}^{(1)}(\omega).\end{aligned}\tag{13}$$

Here $\bar{\Sigma}_{\bar{\sigma}}^{(0)}(\omega) = \bar{F}_{\bar{\sigma}}(\bar{\omega}_{\bar{\sigma}}^0) - \bar{F}_{\bar{\sigma}}^*(-\bar{\omega}^U) + \bar{B}_{\bar{\sigma}}(\omega)$,

$$\bar{F}_{\bar{\sigma}}(\omega) = \sum_{\alpha\mathbf{k}, \alpha'\mathbf{k}'} \bar{V}_{\alpha\mathbf{k}}^* \bar{V}_{\alpha'\mathbf{k}'} \langle \mathbf{c}_{\alpha'\mathbf{k}'\bar{\sigma}}^\dagger \mathbf{c}_{\alpha\mathbf{k}\bar{\sigma}} \rangle g_{\alpha\mathbf{k}}^r(\omega),\tag{14}$$

and

$$\begin{aligned}\bar{B}_{\bar{\sigma}}(\omega) &= -2i\text{Im} \left\{ \sum_{\alpha'\mathbf{k}'} \bar{V}_{\alpha'\mathbf{k}'}^* \langle \mathbf{d}_{\bar{\sigma}}^\dagger \mathbf{c}_{\alpha'\mathbf{k}'\bar{\sigma}} \rangle \right\} \\ &\times \left[\sum_{\alpha\mathbf{k}} |\bar{V}_{\alpha\mathbf{k}}|^2 (g_{\alpha\mathbf{k}}^r(\omega))^2 \right].\end{aligned}\tag{15}$$

In the wide-band limit, $\bar{\Sigma}^{(T)}(\omega) \approx -i\bar{\Gamma}$, and

$$\begin{aligned}\bar{\Sigma}_{\bar{\sigma}}^{(0)}(\omega) &\approx \sum_{\alpha} \frac{\bar{\Gamma}_{\alpha}}{2\pi} \left[\psi \left(\frac{1}{2} + \frac{\bar{\omega}^U + \mu_{\alpha}}{i2\pi k_B T} \right) \right. \\ &\left. - \psi \left(\frac{1}{2} + \frac{\bar{\omega}_{\bar{\sigma}}^0 - \mu_{\alpha}}{i2\pi k_B T} \right) - i\pi \right],\end{aligned}\tag{16}$$

where the Psi function ψ is the logarithmic derivative of the gamma function. Now the self-consistent equation for $\bar{P}_{\bar{\sigma}}(\omega)$ is simplified as

$$\bar{P}_{\bar{\sigma}}(\omega) = \int \frac{d\omega'}{2\pi} \frac{[\bar{\Gamma}_L f_L(\omega') + \bar{\Gamma}_R f_R(\omega')] \bar{G}_{\bar{\sigma}}^{r*}(\omega')}{\omega - \omega' + i0^+},\tag{17}$$

which, together with Eq.(9), gives the dressed retarded Green function $\bar{G}_{\bar{\sigma}}^r$.

As we will see that at zero temperature, not only $\bar{F}_{\bar{\sigma}}(\omega)$, but also $\bar{P}_{\bar{\sigma}}(\omega)$ will diverge logarithmically and then all contribute to the sharp Kondo resonance at each Fermi surface. Therefore, $\bar{P}_{\bar{\sigma}}(\omega)$ should not be ignored as in the previous approaches. [42,43] Generally, this EOM approach works for most cases, however it fails to give the Kondo resonance at the particle-hole symmetric case. For example, when $\bar{\varepsilon}_{\uparrow} = \bar{\varepsilon}_{\downarrow} = -\bar{U}_0/2$, Eqs.(10,11,14) show that $\bar{\omega}_{\bar{\sigma}}^0 = \bar{\omega}^U$, $\bar{P}_{\bar{\sigma}}^*(-\omega) = -\bar{P}_{\bar{\sigma}}(\omega)$, and $\bar{F}_{\bar{\sigma}}^*(-\omega) = -\bar{F}_{\bar{\sigma}}(\omega)$. Therefore the divergent terms in the expression of the retarded Green function are cancelled with each other and then no Kondo resonance will show up. [47] The reason for this limitation is the fact that at the particle-hole symmetry point, the charge fluctuations are completely quenched, therefore the EOM approach can not be applied. [14]

By the Keldysh formula $\bar{G}_{\bar{\sigma}}^{>(<)} = \bar{G}_{\bar{\sigma}}^r \bar{\Sigma}_{\bar{\sigma}}^{>(<)} \bar{G}_{\bar{\sigma}}^a$, in which the the greater (lesser) self-energy is evaluated by the ansatz adopted by Ng [48], the dressed greater and lesser Green functions are obtained as

$$\begin{aligned}\bar{G}_{\bar{\sigma}}^{>}(\omega) &= i([\bar{\Gamma}_L(1 - f_L(\omega)) + \bar{\Gamma}_R(1 - f_R(\omega))] \text{Im} \bar{G}_{\bar{\sigma}}^r(\omega) / \bar{\Gamma}, \\ \bar{G}_{\bar{\sigma}}^{<}(\omega) &= -i[\bar{\Gamma}_L f_L(\omega) + \bar{\Gamma}_R f_R(\omega)] \text{Im} \bar{G}_{\bar{\sigma}}^r(\omega) / \bar{\Gamma}.\end{aligned}\tag{18}$$

Substituting Eq.(18) into Eqs.(5) and (6), one obtains the greater (lesser) Green function and subsequently the spectral function of the SMT.

It is noted that, with the infinity charging energy and zero Zeeman splitting in the equilibrium, our results will recover to the Lacroix's one. [44] Together with the improved canonical transformation, this generalized EOM method will be our framework for investigating the Kondo satellites at the nonequilibrium with finite Zeeman splitting. Although this approach can only give a qualitative description of the shape of the Kondo satellites, it does predict the right peak positions. [26,42,43] For quantitative description of the renormalized properties in the equilibrium or exploring wider parameter space, more accurate methods like the NRG or quantum monte carlo calculations may be appropriate [26–29].

With the spectral function and the lesser Green function given above, the current through the SMT can be calculated via [49,50]

$$J = \sum_{\sigma} \frac{ie}{2\hbar} \int d\omega \{ [f_L(\omega)\Gamma_L - f_R(\omega)\Gamma_R] A_{\sigma}(\omega) + (\Gamma_L - \Gamma_R) G_{\sigma}^{<}(\omega) \}, \quad (19)$$

and the differential conductance can be obtained straightforward as $G = \partial J / \partial V_{bias}$.

4. Spectral Function and Differential Conductance

4.1. spin degenerate case

First, we will discuss the spin degenerate case, i.e., $\varepsilon_{\uparrow} = \varepsilon_{\downarrow} = \varepsilon_0$. The spectral function in the absence of the EPI is plotted in Fig.1(a) for different \bar{U}_0 , which shows that besides the two broad resonant peaks at $\bar{\varepsilon}_0$ and $\bar{\varepsilon}_0 + \bar{U}_0$, there will be a sharp Kondo resonance developed at $\mu_{L(R)}$. By increasing \bar{U}_0 , as can be observed from the inset of Fig.1(a), this Kondo resonant peak can be tuned more and more asymmetric, which is a manifestation of the particle-hole asymmetry of the SMT.

When the electron-phonon interaction is turned on, as shown in Fig.1(b), the Kondo peak will be split into a set of phonon satellites spaced by multiple of phonon frequency. When the system is driven out of equilibrium by applied a bias voltage, the main Kondo peak will be split into two weakened peaks pinning at Fermi levels of the left and right lead, respectively, and the phonon Kondo satellites will also be split into two corresponding sub-sets. These results well agree with previous works, which validates the present framework [24,25,42,43].

The underlying physics about how and why the Kondo satellites develop in such a way can be intuitively understood with the help of Fig.2. As illustrated by Fig.2(a1), a local hole state in the SMT exchanges with the excited holes at leads below the Fermi energy μ to form a Kondo spin-singlet. When an electron hops to the local state by emitting a phonon, as shown in Fig.2(a2), only the holes with energy below $\mu - \hbar\omega_0$ can exchange with the local hole, because the phonon absorption is unavailable at very low temperature and the energy conservation law must be satisfied in the interaction

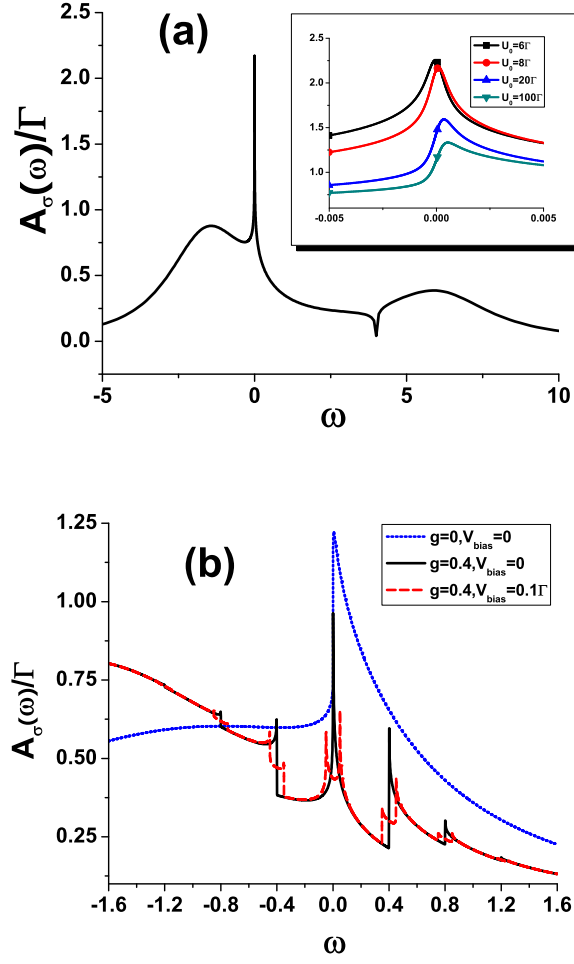


Figure 1. (color online) The spectral functions of the spin degenerate local electrons, i.e., A_σ , with (a) and without (b) the EPI. The parameters used in (a) are: $\mu_L = \mu_R = 0.0$, $\varepsilon_0 = -2\Gamma$, and $U_0 = 8\Gamma$, $V_{bias} = 0$. The parameters used in (b) are $(\mu_L + \mu_R)/2 = 0$, $\varepsilon_0 = -2.5\Gamma$, $k_B T = 2 \times 10^{-4}\Gamma$, $U_0 = 100\Gamma$, $\hbar\omega_0 = 0.4\Gamma$. Other parameters have been shown explicitly in each figures.

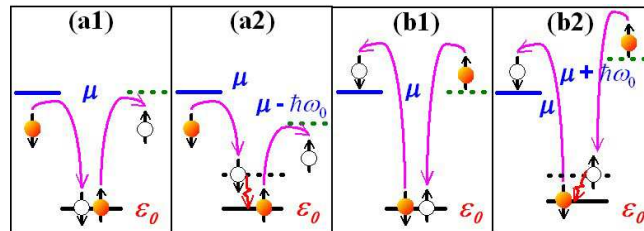


Figure 2. (color online) Schematic illustration for the spin exchange processes associated with the formation of the Kondo satellites.

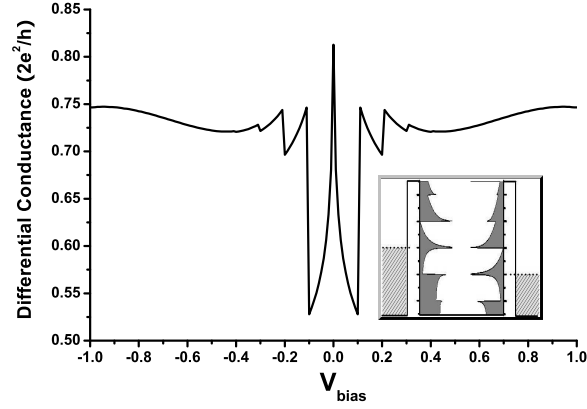


Figure 3. The differential conductance for spin degenerate case as a function of the bias voltage. Here $\bar{\epsilon}_0 = -2.5\Gamma$, $g = 0.5$, $k_B T = 2 \times 10^{-4}\Gamma$, $U_0 = 100\Gamma$, and $\hbar\omega_0 = 0.1\Gamma$. As an illustration, the inset shows the origin of the first Kondo phonon-satellite peak schematically.

process. Thus a phonon-satellite peak at $\mu - \hbar\omega_0$ appears in the density of states or tunneling spectra. Similarly, a spin-singlet consisting of a localized electron and excited electrons above μ is depicted in Fig.2(b1), and only the electrons above $\mu + \hbar\omega_0$ can exchange with the local electron if the hopping processes are accompanied by emitting a phonon as shown in Fig.2(b2), which will give rise to the satellite peak at $\mu + \hbar\omega_0$. That means although both processes shown in Fig.2(a1) and Fig.2(b1) contribute to the main Kondo peak, they can be distinguished by their Kondo satellites, namely, the contributions of each type of exchange processes to the Kondo peak can be picked out in principle by comparing with the satellites on each sides of the main peak.

Fig.1(b) also shows the satellites on different sides of the Kondo main peak may take on apparent sharp asymmetric lineshapes. The reason for these sharp feature lies in the sharp Fermi distributions in the leads at very low temperature, where the electron excitations and the hole excitations are separated from each other sharply by the Fermi surface. For example, the phonon-assisted spin exchange processes mentioned above have the sharp energy boundaries as $\mu_{L(R)} \pm n\omega_0$, therefore they may result in the sharp features at $\omega = \mu_{L(R)} \pm n\omega_0$ as shown in Fig.1(b). Besides, if the localized level is broadened so that there is a finite density of states around $\mu_{L(R)}$, the electron can also bypass the SMT via the phonon-assisted resonant tunneling processes. According to our previous studies, [21] these phonon-assisted resonant tunneling processes can result in the phonon sidebands at $\omega = \bar{\epsilon}_0 \pm n\omega_0$, which also exhibit some sharp asymmetric lineshapes at $\omega = \mu_{L(R)} \pm n\omega_0$ under extremely low temperature. These structures superpose over the Kondo-phonon-satellites, jointly responsible for the apparent sharp asymmetric peaks observed in Fig.1(b).

The nonlinear differential conductance versus the bias voltage, i.e., $G(V_{bias})$, is plotted in Fig.3 for very low temperature, where G reaches a peak value at $V_{bias} = 0$

and then decreases rapidly as V_{bias} increases. This zero-bias anomaly is usually regarded as the experimental evidence for the Kondo effect in the quantum dot systems. When $eV_{bias} = n\hbar\omega_0$, there are some Kondo-phonon-satellite peaks show up, as evidenced by the very recent experiments. [15–17] According to the general understanding, in the non-EPI case the bias voltage plays a role similar to temperature, which means the differential conductance decreases logarithmically as V_{bias} increases, [51] one may wonder here why the apparent sharp asymmetric features of the Phonon-Kondo-peaks in Fig.3 have not been smoothed out by bias voltage. It is because the Fermi distributions in the leads have sharp Fermi surfaces at very low temperature, the sharp features of the spectral function, as shown in Fig.1(b), can still be preserved even for finite bias voltage. As illustrated in the inset of Fig.3, once an asymmetric peak in the spectral function matches one of the Fermi levels, a sharp asymmetric differential conductance peak will appear. Therefore, the apparent sharp asymmetric features in $G(V_{bias})$ are just the manifestations of the asymmetric lineshapes of the spectral function, which contain both contributions from the phonon-assisted Kondo processes and the phonon-assisted resonant tunneling processes as well. These sharp asymmetric features can only be smoothed out with the increasing temperature.

It is worth pointing out the resemblances between our spin degenerate results and those by the real-time diagrammatic formulation [24, 25] or the generalized Schrieffer-Wolff transformation [30], where the discontinuous and asymmetric lineshape features of the Kondo-phonon-satellites in the spectral function or the differential conductance can also be observed, but have not yet been clearly pointed out and properly explained previously.

4.2. finite Zeeman splitting case

Now let us take a look at the spin non-degenerate case, where a Zeeman splitting of Δ for the localized level may be induced by a local magnetic field, i.e. $\varepsilon_{\uparrow} = \varepsilon_0 + \Delta/2$ and $\varepsilon_{\downarrow} = \varepsilon_0 - \Delta/2$.

Without the EPI, our calculation for the spin-splitting case shows that, compared to the spin-degeneracy case, the Kondo peak in the spin-resolved spectral function $A_{\uparrow}(\omega)$ (or $A_{\downarrow}(\omega)$) generally decreases in magnitude and shifts away from μ by Δ ($-\Delta$), which agrees with previous researches. [24–29, 42, 43] When the EPI turns on, as shown in Fig.4(a), the phonon satellite structure may develop in a distinct way, that is, for moderate Zeeman splitting only the satellites above (below) the main peak appear in $A_{\uparrow}(\omega)$ ($A_{\downarrow}(\omega)$).

This peculiar feature in the spin-resolved spectral function stems from the interplay between the EPI and Kondo effect in the presence of the finite spin-splitting. It also manifests itself in the differential conductance. As shown in Fig.4(b), there is no satellite appearing in the region $\mu - \Delta < eV_{bias} < \mu + \Delta$, which is generally true as long as the system is at very low temperature. According to our simple picture above (*cf* Fig.2), it is easy to understand.

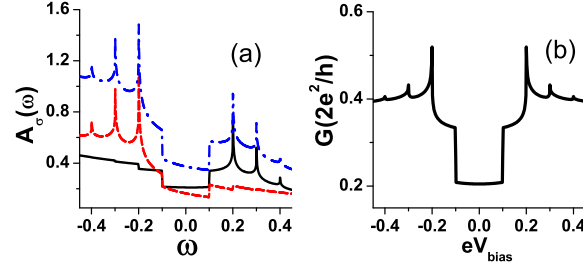


Figure 4. (color online) The calculated total (blue dash dot line) and spin-resolved (black solid line for spin up, and red dash line for spin down) spectral functions in the equilibrium (a), and the nonlinear differential conductance (b) in the presence of finite Zeeman splitting. Here $\bar{\varepsilon}_0 = -2.5\Gamma$, $g = 0.6$, $k_B T = 2 \times 10^{-4}\Gamma$, $U_0 = 100\Gamma$, $\hbar\omega_0 = 0.1\Gamma$, and $\Delta = 0.2\Gamma$.

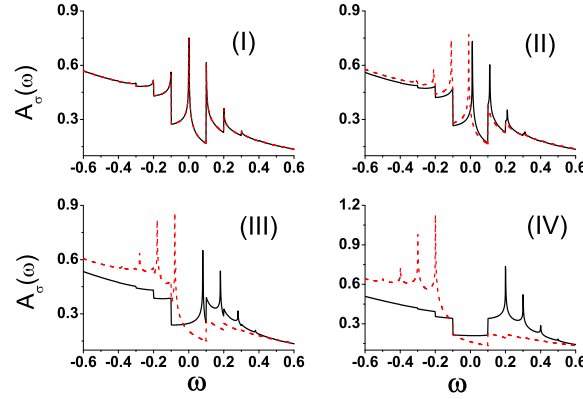


Figure 5. (color online) The spin-resolved spectral function (black solid line for spin up, red dash line for spin down component) for different Zeeman splitting: (I) $\Delta = 0$, (II) $\Delta = 0.01\Gamma$, (III) $\Delta = 0.08\Gamma$, and (IV) $\Delta = 0.2\Gamma$. Other parameters are taken as $V_{bias} = 0$, $\bar{\varepsilon}_0 = -2.5\Gamma$, $g = 0.6$, $U_0 = 100\Gamma$, and $\hbar\omega_0 = 0.1\Gamma$.

The spin-resolved spectral functions for four different Zeeman splitting values are plotted in Fig.5, demonstrating that when the Zeeman splitting turns on, the overall Kondo peaks in the spin down spectral function shift towards the low energy, while those for spin up make a blue shift. The Kondo satellites above (below) the main peak in the spin down (up) spectral function decrease significantly as the Zeeman splitting is increased, then disappear when the Δ exceeds the line-width of the Kondo peak which is proportional to the Kondo temperature $k_B T_K$. However, for larger splitting, the main Kondo peak itself will be much suppressed, so that this spin-dependence of the Kondo phonon satellites will not be resolved at all.

To understand how this pattern develops, it is helpful to recall that the satellite on different sides of the main peak is associated with different spin exchange process as depicted in Fig.2. This peculiar pattern for finite Zeeman splitting indicates that

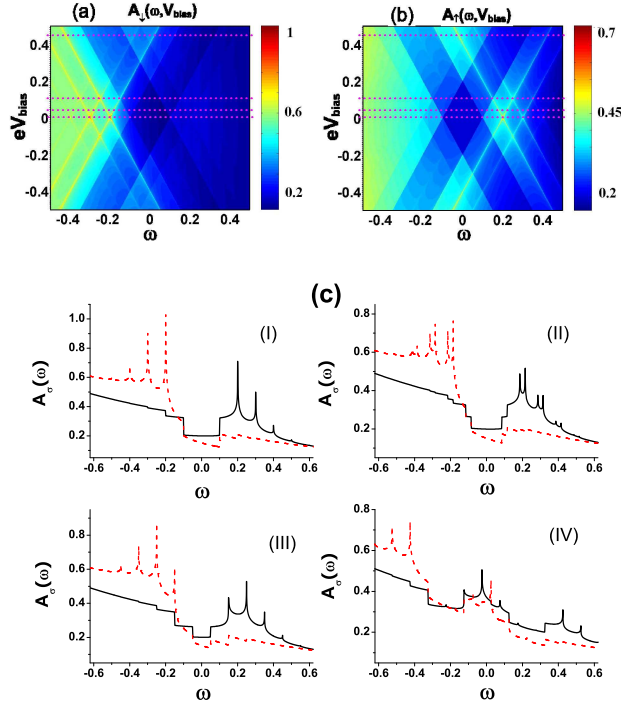


Figure 6. (color online) Maps for the spin up (a) and spin down (b) spectral functions as functions of ω and eV_{bias} . The sections are plotted in (c) for four typical bias voltages: (I) $eV_{bias} = 0$, (II) $eV_{bias} = 0.03\Gamma$, (III) $eV_{bias} = 0.1\Gamma$, (IV) $eV_{bias} = 0.45\Gamma$. Here $\Delta = 0.2\Gamma$, $\varepsilon_0 = -2.5\Gamma$, $g = 0.6$, $U_0 = 100\Gamma$, and $\hbar\omega_0 = 0.1\Gamma$.

the dominant contribution to the main peak in $A_\uparrow(\omega)$ comes from the coupling of the local state with the excited conduction electron states, while for $A_\downarrow(\omega)$ the dominant contribution comes from the coupling with the excited hole states. If $\Delta = 0$, as illustrated in Fig.2, both spin exchange processes contribute to the Kondo main peak. When Δ starts to increase, both spin exchange processes decay in magnitude, but at different rates. When Zeeman splitting increases further, it would be possible that while one spin exchange process remains finite, the other is already totally suppressed. This results in the spin separation of the Kondo phonon satellites in the spectral function. However, when $\Delta \gg k_B T_K$, so that both processes are unlikely to happen and finally the Kondo peaks are quenched.

The spin down (up) spectral function for fixed Zeeman splitting is shown in Fig.6(a) (Fig.6(b)) as function of ω and V_{bias} , in which the highlighting cross lines correspond to the Kondo satellites. For explicitly, the sections at the four typical bias voltages marked by the dash lines in Fig.6(a) and Fig.6(b) are also plotted in Fig.6(c), respectively. One can clearly see that, when the bias voltage turns on, each Kondo peak is separated into two sub-peaks related to two Fermi levels, respectively. These two sub-sets of Kondo satellites separate from each other further when V_{bias} increases, resulting in the peculiar pattern as shown in Fig.6(c).

5. Conclusion

In summary, taking advantage of the improved treatment of the electron-phonon interaction and the extended equation of motion approach, we have systematically investigated the Kondo effect in the SMT in the presence of the electron-phonon interaction, finite bias voltage, and Zeeman splitting. The phonon-Kondo satellites observed in the recent SMT transport experiments [15–17] have been confirmed and explained by our results. Moreover, peculiar patterns of phonon-Kondo satellites in the spectral function as well as the differential conductance have also been predicted and explained by a clear physics picture. Although it is the interplay between the EPI and Kondo processes that discussed here, the physics picture and the theoretical calculation presented here may also be applicable to some other cases. For instance, the interplay of electronic internal excitations and the Kondo processes can also manifest themselves in some parallel Kondo satellites. [8]

Acknowledgments

The authors thank the helpful discussions with H. Zhai, Z. G. Zhu, F. Ye, C. X. Liu and R. B. Liu. This work is supported by the NSF of China (Grant No. 10374056, 10574076), the MOE of China (Grant No. 200221), and the Program of Basic Research Development of China (Grant No. 2001CB610508).

References

- [1] T. K. Ng and P. A. Lee 1988 *Phys. Rev. Lett.* **61** 1768
- [2] L. I. Glazman and M. E. Raikh 1988 *JETP Lett.* **47** 452
- [3] A. C. Hewson 1997 *The Kondo Problem to Heavy Fermions* (Cambridge: Cambridge University Press)
- [4] S. M. Cronenwett, T. H. Oosterkamp and L. P. Kouwenhoven 1998 *Science* **281** 540
- [5] D. G. Gordon, H. Shtrikman, D. Mahalu, D. A. Magder, U. Meirav and M. A. Kastner 1998 *Nature (London)* **391** 156
- [6] J. Schmid, J. Weis, K. Eberl and K. v. Klitzing 1998 *Physica B (Amsterdam)* **256** 182
- [7] W. G. v. d. Wiel, S. D. Franceschi, T. Fujisawa, J. M. Elzerman, S. Tarucha and L. P. Kouwenhoven 2000 *Science* **289** 22
- [8] J. Nygård, D. H. Cobden, and P. E. Lindelof 2000 *Nature (London)* **408** 342
- [9] J. Park, A.N. Pasupathy, J. I. Goldsmith, C. Chang, Y. Yalsh, J. R. Petta, M. Rinkoskl, J. P. Sethna, H. D. Abruña, P. L. McEuen and D. C. Ralph 2002 *Nature (London)* **417** 722
- [10] W. Liang, M. P. Shores, M. Bockrath, J. R. Long and H. Park 2002 *Nature (London)* **417** 725
- [11] A. N. Pasupathy, R. C. Bialczak, J. Martinek, J. E. Grose, L. A. K. Donev, P. L. McEuen and D. C. Ralph 2004 *Science* **306** 86
- [12] A. Kogan, S. Amasha and M. A. Kastner 2004 *Science* **304** 1293
- [13] J. Martinek, Y. Utsumi, H. Imamura, J. Barnaś, S. Maekawa, J. König and G. Schön 2003 *Phys. Rev. Lett.* **91** 127203
- [14] M. S. Choi, D. Sanchez and R. López 2004 *Phys. Rev. Lett.* **92** 056601
- [15] L.H. Yu and D. Natelson 2004 *Nano Letters* **4** 79
- [16] L.H. Yu and D. Natelson 2004 *Nanotechnology* **15** S517

- [17] L. H. Yu, Z. K. Keane, J. W. Ciszek, L. Cheng, M. P. Stewart, J. M. Tour and D. Natelson 2004 *Phys. Rev. Lett.* **93** 266802
- [18] H. Park, J. Park, A. K. L. Lim, E. H. Anderson, A. P. Alivisatos and P. L. McEuen 2000 *Nature (London)* **407** 57
- [19] J. Koch and F. V. Oppen 2005 *Phys. Rev. Lett.* **94** 206804
- [20] M. Galperin, M. A. Ratner and A. Nitzan 2004 *Nano Letters* **4** 1605
- [21] Z. Z. Chen, R. Lü and B. F. Zhu 2005 *Phys. Rev. B* **71** 165324
- [22] K. Yosida 1966 *Phys. Rev.* **147** 223
- [23] G. D. Mahan 1990 *Many-Particle Physics* (New York and London: Plenum press, 2nd Ed.) p 967
- [24] J. Köning, H. Schoeller and G. Schön 1996 *Phys. Rev. Lett.* **76** 1715
- [25] J. Köning, J. Schmid and H. Schoeller 1996 *Phys. Rev. B* **54** 16820
- [26] A. C. Hewson and D. Meyer 2002 *J. Phys: Condens. Matter* **14** 427
- [27] P.S. Cornaglia, H. Ness and D. R. Grempel 2004 *Phys. Rev. Lett.* **93** 147201
- [28] P.S. Cornaglia, D.R. Grempel and H. Ness 2005 *Phys. Rev. B* **71** 075320
- [29] P. S. Cornaglia and D. R. Grempel 2005 *Phys. Rev. B* **71** 245326
- [30] J. Paaske and K. Flensberg 2005 *Phys. Rev. Lett.* **94** 176801
- [31] H. C. Lee and H. Y. Choi 2004 *Phys. Rev. B* **70** 085114
- [32] V. Aji, J. E. Moore and C. M. Varma 2003 *Preprint cond-mat/0302222*
- [33] J. H. Han 2004 *Preprint cond-mat/0405477*
- [34] A. Mitra, I. Aleiner and A. J. Millis 2004 *Preprint cond-mat/0409248*.
- [35] S. Kubatkin, A. Danilov, M. Hjort, J. Cornil, J. L. Brédas, N. Stuhr-Hansen, P. Hedegård and T. Bjørnholm 2003 *Nature (London)* **425** 698
- [36] U. Lundin and R.H. McKenzie 2002 *Phys. Rev. B* **66** 075303
- [37] David M. T. Kuo and Y. C. Chang 2002 *Phys. Rev. B* **66** 085311
- [38] J. X. Zhu and A. V. Balatsky 2003 *Phys. Rev. B* **67** 165326
- [39] G. D. Mahan 1990 *Many-Particle Physics* (New York and London: Plenum press, 2nd Ed.) p 533
- [40] A. C. Hewson and D. M. Newns 1979 *J. Phys. G: Solid st. Phys.* **12** 1665
- [41] A. C. Hewson and D. M. Newns 1980 *J. Phys. C: Solid St. Phys.* **13** 4477
- [42] Y. Meir, N. S. Wingreen and P. A. Lee 1993 *Phys. Rev. Lett.* **70** 2601
- [43] R. Świrkowicz, J. Barnaś and M. Wilczyński 2003 *Phys. Rev. B* **68** 195318
- [44] C. Lacroix 1981 *J. Phys. F: Metal Phys.* **11** 2389
- [45] H. Huag and A. P. Jauho 1998 *Quantum Kinetics in Transort and Optics of Semiconductors* (Springer-Verlag)
- [46] After submitting our manuscript, a closed related work by V. Kashcheyevs etc. with a similiar (with a little different truncate approximation) EOM derivations of the Green functions appears, the details of the derivation can be found in their appendix. V. Kashcheyevs, A. Aharony, and O. E. Wohlman 2006 *Phys. Rev. B* **73** 125338
- [47] The drawback of the EOM at the particle-hole symmetric point has also been dicussed in Ref. [46].
- [48] T. K. Ng 1996 *Phys. Rev. Lett.* **76** 487
- [49] Y. Meir and N. S. Wingreen 1992 *Phys. Rev. Lett.* **68** 2512
- [50] A. -P. Jauho, N. S. Wingreen and Y. Meir 1994 *Phys. Rev. B* **50** 5528
- [51] J. Appelbaum 1966 *Phys. Rev.* **17** 91